CHANGES IN THE SEAWATER SALINITY–OXYGEN ISOTOPE RELATION BETWEEN LAST GLACIAL AND PRESENT: SEDIMENT CORE DATA AND OGCM MODELLING

Paleoclimates, 1998, Vol. 2(2-3), pp. 101-131

Christian Schäfer-Neth
Research Centre Ocean Margins, University of Bremen, Germany
email: csn@uni-bremen.de

ABSTRACT

The presently available paleotemperature data implies large ice-free areas in the Greenland-Iceland-Norwegian Seas during the Last Glacial Maximum 21 600 yr BP. From these temperatures and the independent measurements of oxygen isotope ratios of fossil foraminiferal shells, glacial sea surface salinities could be computed, if the glacial relation between salinity and water isotope ratio was known. For this study, a three-dimensional numerical ocean circulation model was employed to investigate the possible shape of this still not precisely known relation, and to reconstruct a physically consistent scenario of the northern North Atlantic for the glacial summer. This scenario turned out to be quite similar to modern winter conditions, whereas the required salinity vs. oxygen isotope relation of this time must have been very different from its modern counterpart.

1 INTRODUCTION

One essential task of paleoceanographic reconstructions is to determine the sea surface temperatures (T) and salinities (S) for a former timeslice from the deep sea sedimentological record. As far as the high latitudes in general and more specifically the northern North Atlantic is concerned, the most important parameter is S, since it controls possible regions and intensity of deep water formation and therefore has a major impact on the global thermohaline circulation. During the last few years, the methodological and analytical tools used for transforming sediment core data into oceanographic variables, such as ^{14}C dating, mass spectrometry, and transfer functions, have continuously been improved. However, the errors of T and S reconstructed from a single sediment core are still in the range of about 1 $^{\circ}$C (Pflaumann *et al.*, 1996) and 1 psu (Schäfer-Neth, 1994) despite all recent advances. T and S changes of these magnitudes can have quite severe effects on the circulation system and the formation of water masses (Haupt *et al.*, 1994, 1995) so that it is impossible to verify or assess a paleoceanographic reconstruction by assessing the temperature and salinity errors. For narrowing the bandwidth of the reconstructed parameters, further restrictions must be employed. For example, Zahn and Mix (1991) used the requirement of stable stratification.

In the work presented here, SCINNA (= "Sensitivity and Circulation of the Northern North Atlantic"), a three-dimensional ocean general circulation model is used as an extensive set of

physical constraints to filter out consistent data sets from the possible ones. In some sense, this application of a circulation model means looking at natural causalities from a reversed point of view. The real ocean is driven by the combined effects of thermal, haline, and wind forcing and shows a single specific circulation system and water mass distribution. In turn, when forcing the numerical model with different T and S fields, the resulting circulation must be consistent with both. If there are contradictions, for example a salinity-driven current conflicting with the temperature field, something must have been wrong with the T and/or S reconstructions. Of course, the same argument applies to the wind forcing. Thus the circulation model helps to improve the transfer techniques and to refine the paleoceanographic reconstruction.

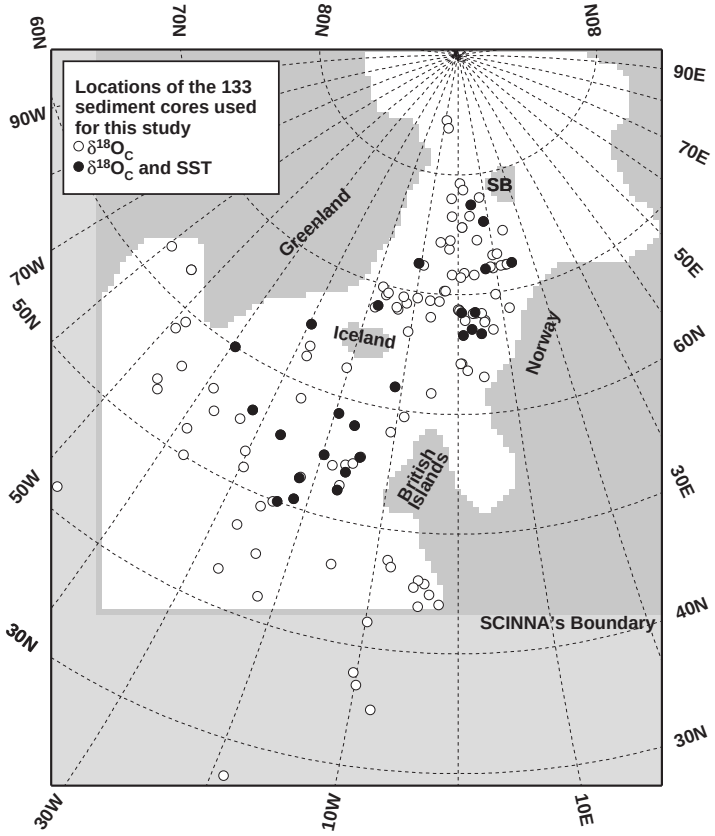

Figure 1: *Locations of the sediment cores employed for this work. Empty circles: cores with measurements of foraminiferal $\delta^{18}O_C$, filled circles: cores with both $\delta^{18}O_C$ measurements and independent T estimates.*

The objective of the present study is: (i) to compile a physically consistent scenario of the northern North Atlantic during the Last Glacial's summer (18 000 ^{14}C, 21 600 calendar years BP), based on the T reconstructions from faunal assemblages (Pflaumann *et al.*, 1996) and $\delta^{18}O_C$, the oxygen isotope ratios measured at fossil shells of the planctonic forminiferans *Neogloboquadrina pachyderma sin.* and *Globigerina bulloides*, and (ii) to yield new insights whether and to what extent the relationship between S and oxygen isotopes may have changed during geological history. The interrelations between sediment core data and derived oceanographic parameters are discussed in conjunction with different approaches for calculating paleo-salinities. Then, the different methods for determining paleo-salinity will be assessed according to the model results obtained by forcing SCINNA with the different salinity reconstructions.

2 DATA AND MODEL

2.1 Data Base

This work was based on a total of 133 (Fig. 1) cores with $\delta^{18}O_C$ measurements from various sources (Table 1). For 25 of these cores, glacial sea surface temperatures have been indepently estimated (Weinelt *et al.*, 1996; Table 1, '96 T_{rek} data). The data represent an average over 3000 years (18–15 kyr ^{14}C BP) of stable glacial conditions that are easily identified in the sedimentary data (Weinelt *et al.*, 1996). The subsequent climatic changes indicated in the records by Heinrich and other deglaciation events (e. g. Bond and Lotti, 1995; Sarnthein *et al.*, 1995) are not considered here. From these sediment core data, the sea surface T and S fields for driving SCINNA have been derived in three steps (Fig. 2):

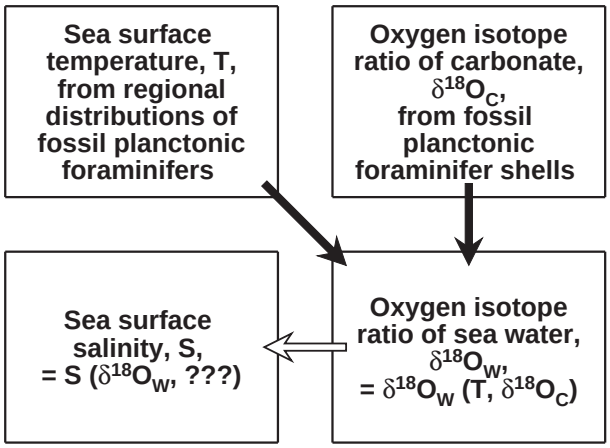

Figure 2: *Interrelation between the two parameters obtained from sediment core measurements (T and $\delta^{18}O_C$, top row) and those needed for forcing the model (T and S, left column). Black arrows indicate the empirical relationships given by the paleotemperature equation (2). The unknown glacial S-$\delta^{18}O_W$-relation is symbolized by the white arrow.*

First, the core-based temperatures (Fig. 3, filled circles) were supplemented by the CLIMAP (1981) summer reconstruction south of 50N (open circles). To fill in the remaining gaps, freezing conditions (-1.9 $^\circ$C) in the polar ocean, in the Barents Sea and at the northern end of the Labrador Sea were assumed, with a smooth increase to 2 $^\circ$C at the southern coast of Greenland and the southern end of the Labrador Sea (triangles). By triangulation (Wessel and Smith, 1991) and smoothing, these punctual T data were interpolated to every model grid point (Fig. 3, isolines). The points outside the model area were included in the triangulation to avoid unrealistic gradients at the boundaries. The resulting field has many resemblances to modern winter conditions, such as the largely ice-free GIN Seas, and indications for an inflow into the Norwegian Sea over the Iceland-Færøe-Scotland Ridge. This temperature field was used for forcing all of the experiments described here.

Second, the gridded temperatures were interpolated to the locations of the sediment cores with $\delta^{18}O_C$ measurements (Table 1, T_{int}). By means of equations (2) and (3) that are introduced in the following section, the water oxygen isotope ratio $\delta^{18}O_W$ was computed (Fig. 2, black

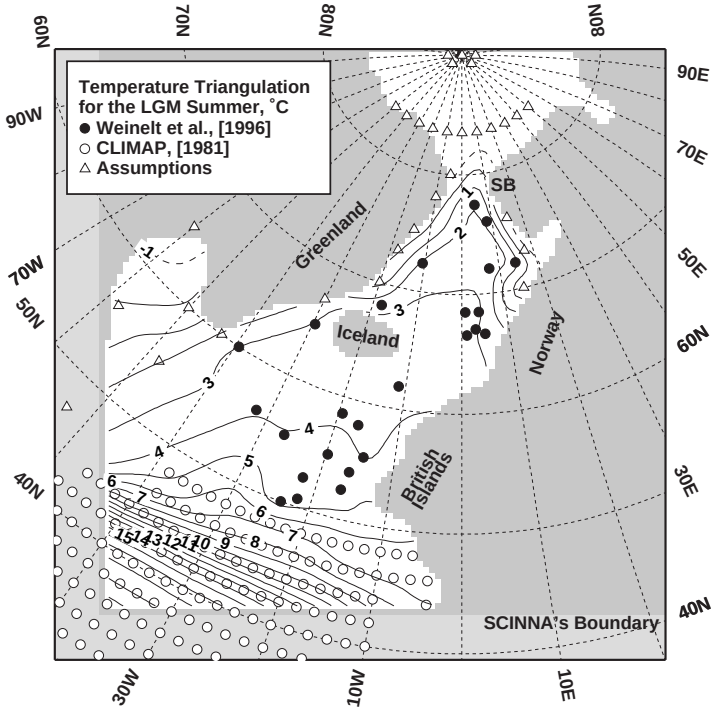

Figure 3: *Glacial summer sea surface temperature triangulated from the core-based T estimates (filled circles), parts of the CLIMAP (1981) reconstruction (open circles), and assumptions (triangles, see text). Contour interval = 1 ˚C.*

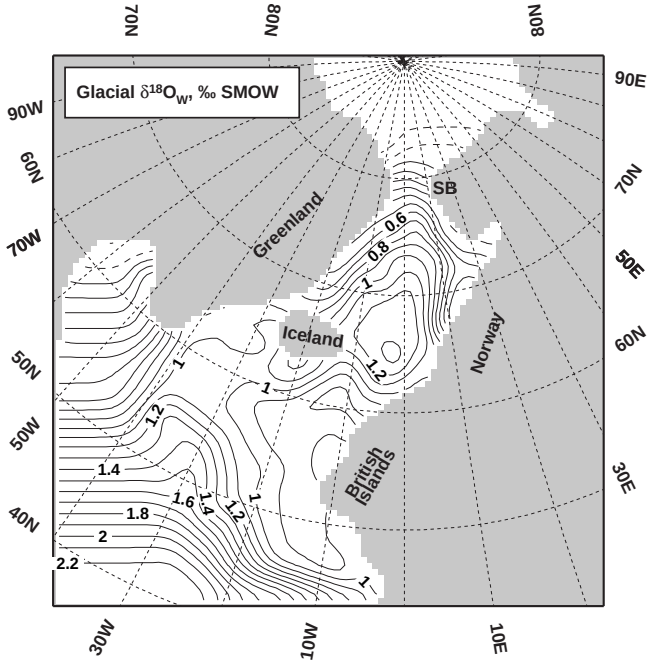

Figure 4: *Glacial distribution of the water oxygen isotopic composition, computed from the $\delta^{18}O_C$ data and the triangulated T field. Contour interval = $0.1^0/_{00}$.*

arrows) for each core from T_{int} and $\delta^{18}O_C$ (Table 1, $\delta^{18}O_W$). In case of *N. pachyderma sin.* data, the 0–50 m version of equation (3) was used, because the resulting model forcing was applied to the whole uppermost model level of 50 m thickness. Triangulation and smoothing of the core-based $\delta^{18}O_W$ then yielded the distribution of $\delta^{18}O_W$ shown in Fig. 4, covering the

whole model area. Its main features are the maximum up to $1.3^0/_{00}$ in the Norwegian Sea, the minimum of 0.8–$0.9^0/_{00}$ off the British Islands, and a tongue with values $> 1.2^0/_{00}$ extending northward along 30W. Core CH 69-09 at 47.35W/41.75N was not used for triangulation. Its $\delta^{18}O_W$ value of $1.63^0/_{00}$ would have introduced sharp fronts along SCINNA's western boundary by bending the isolines $< 1.6^0/_{00}$ northward and those $> 1.6^0/_{00}$ to the south, thus causing strong salinity-driven currents inconsistent with the wind-driven circulation. Unfortunately, CH 69-09 is the only core available in this area, and its isotope ratio could not be assessed by other measurements. Therefore it was simply omitted.

Third, the interpolated $\delta^{18}O_W$ field and various assumptions for the glacial S-$\delta^{18}O_W$-Relation (Fig. 2, white arrow) were employed to compute different glacial sea surface salinity distributions. By driving SCINNA with these S distributions and the T filed described above, the consistency of the salinity reconstructions was checked. The different salinity fields are discussed in the final section in conjunction with the respective model results.

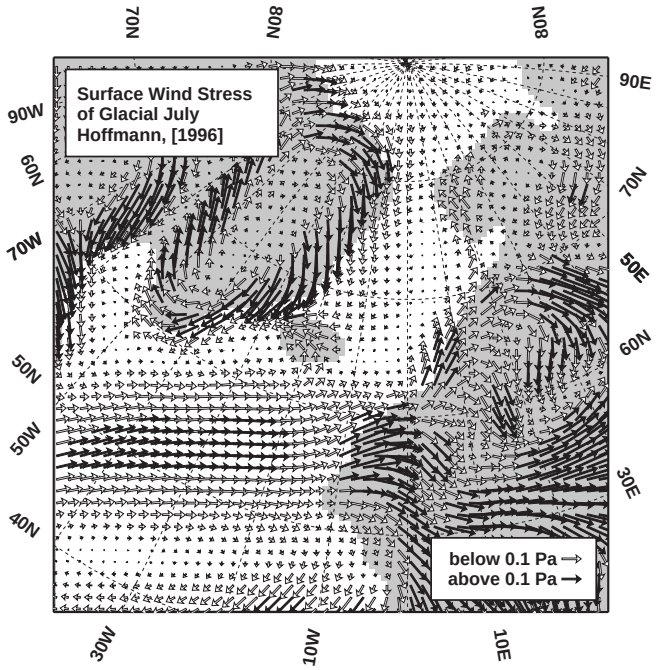

Figure 5: *Glacial July surface wind stress (Hoffmann, 1996, pers. comm.). Only one vector in two is displayed for clarity. Length of scaling vectors = 0.1 Pa.*

The wind field (Fig. 5) used for all the experiments was taken from the July wind stress of a glacial reconstruction with the ECHAM-T42 atmospheric model that was run (Hoffmann, 1996, pers. comm.) with an earlier, slightly different sea surface T reconstruction (Schulz, 1994) of the ice-free GIN Seas (cf. Table 1, '94 T_{rek} data).

2.2 SCINNA

SCINNA is a three-dimensional prognostic Ocean General Circulation Model employing the primitive equations, based on the Modular Ocean Model by Pacanowski *et al.* (1993). To min-

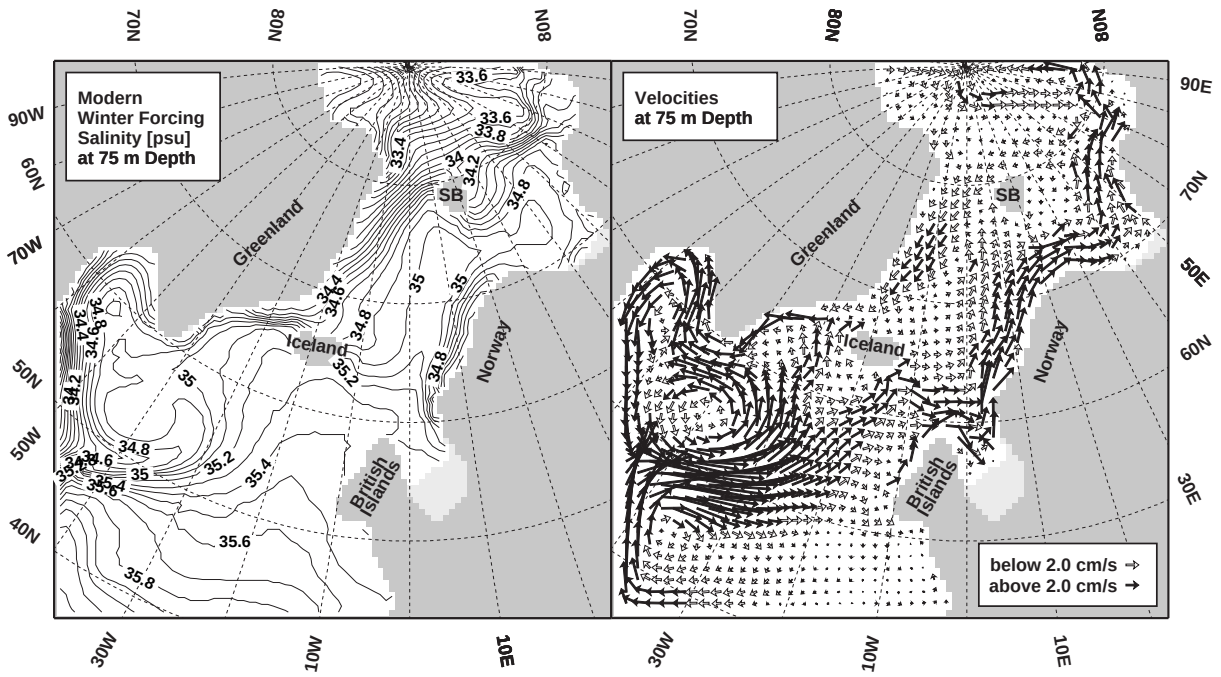

Figure 6: *Salinities and velocities at 75 m depth obtained by forcing SCINNA with modern winter surface T, S (Levitus, 1982; Dietrich, 1969), ice (Wadhams, 1986) and wind (Hellerman and Rosenstein, 1983). The model reproduces the modern salinity distribution and circulation patterns very well. Most noticeable are the salty inflow into and the low-salinity outflow from the GIN seas and the Labrador, Irminger, and North Atlantic Currents. Contour interval = 0.1 psu, scaling vectors = 2 cm/s (Only one vector in two is shown for clarity).*

imize the convergence of meridians and the associated numerical difficulties, it is written not in conventional geographical coordinates but in a rotated spherical system where the model's north pole is located at 180W/30N. The model domain is resolved with 0.5 degrees ($\approx$ 55 km) horizontally and vertically by 17 levels from 50 m thickness at the top to 1000 m at the bottom of the deepest basins, thus allowing a realistic representation of bottom topography. A complete description can be found in Haupt *et al.* (1994). For validating SCINNA, the model was driven with the modern temperature, salinity, and wind stress fields at the sea surface (Haupt *et al.*, 1994, 1995), and both the modern watermass distribution and circulation system, comprising the Norwegian, East Greenland, Labrador, Irminger, and North Atlantic Currents, were very well reproduced in these experiments (Fig. 6).

The model domain includes the Greenland-Iceland-Norwegian (GIN) Seas and their adjacent basins (Fig. 7). The bottom topography was interpolated from the ETOPO5 (1986) data set and further modified to take into account the glacial 100 m sea level lowering (Fairbanks, 1989) and the shelf glaciation down to typically 200 m depth with respect to the glacial sea level (CLIMAP, 1981; Lehman *et al.*, 1991; Mienert *et al.*, 1992). This LGM topograhpy exhibits narrower and shallower straits between Greenland, Iceland, and Scotland than the modern. Further on, the Barents and North Sea are not present any more.

SCINNA's southern and northern limits pose a problem. Ideally, open boundaries should be

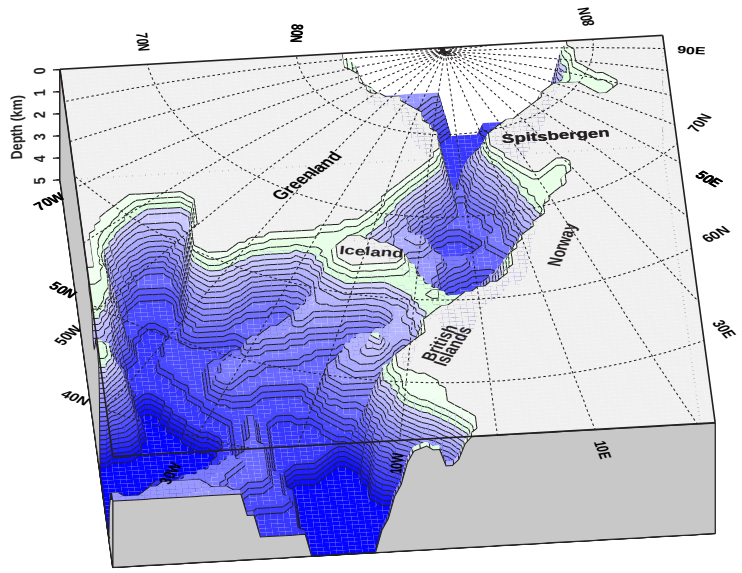

Figure 7: *SCINNA's extent and LGM topography shown in 3-D from the southwest. Contour interval = 50 m.*

implemented along these margins to include the effects of the global ocean. However, the main purpose of the model is to aid paleo-reconstructions, and for former time slices the necessary specification of momentum, vorticity, mass, heat, and salt transports across the boundaries cannot be accomplished. All we have up to now are estimates of (mainly surface) temperatures and salinities. Therefore I resort to restoring zones 5 gridpoints ($\approx$ 275 km) wide that can be imposed along the artificially closed boundaries. However, in test experiments based on the modern temperatures and salinities the circulation in the GIN Seas and the overflows into the North Atlantic turned out to be very insensitive to the presence or absence of the restoring zones. Therefore and due to the lack of three-dimensional glacial T and S, the LGM studies presented here were performed without restoring.

At the surface, the model can be driven alternatively by restoring to specified sea surface temperatures and salinities or by the fluxes of heat and freshwater. Again, because only T and S are available for the work presented here, the restoring method is used with a restoring time scale of 30 days. Flux boundary conditions are useful e. g. for studying meltwater inputs during deglaciation phases: The freshwater flux may be diagnosed from a given state of the model and be modified by adding meltwater inputs along the coasts (Schäfer-Neth and Stattegger, 1996).

3 PALEO-SALINITIES

Sea surface salinity and oxygen isotopic composition of the surface waters ($\delta^{18}O_W$) are linked together by the impacts of evaporation and precipitation (white arrow, Fig. 2), and in the modern ocean both parameters are well correlated by

$$S = S_0^{rec} + \mu^{rec}\,\delta^{18}O_W, \quad \text{with} \quad S_0^{rec} = 34.52 \text{ psu}, \quad \mu^{rec} = 1.792 \tag{1}$$

(GEOSECS, 1987). By taking into account only the GEOSECS data from the uppermost 250

m of the Atlantic, one finds the slightly modified coefficients $S_0^{rec} = 34.66$ psu and $\mu^{rec} = 1.658$ (dashed line, Fig. 8). If we knew both S_0^{LGM} and μ^{LGM} (Fig. 2, "???"), we could easily determine S for the LGM, since $\delta^{18}O_W$ is documented in the oxygen isotope ratio of fossil planctonic foraminiferal shells ($\delta^{18}O_C$), and can be computed by means of the paleotemperature-equation

$$\delta^{18}O_W = \delta^{18}O_C + \varepsilon - 21.9 + \sqrt{310.61 + 10T_c}, \tag{2}$$

(Epstein *et al.*, 1953; Shackleton, 1974) (black arrows, Fig. 2), with $\varepsilon = 0.27$ accounting for the different standards SMOW and PDB, against which $\delta^{18}O_W$ and $\delta^{18}O_C$ are commonly expressed. T_c denotes the calcification temperature, the temperature of the water the foraminifer lived in while building its shell. T_c depends on the sea surface temperature T and the depth habitat of the foraminifers, and for some species simple relations are known:

$$\begin{array}{lll} \textit{Neogloboquadrina pachyderma sinistral} & & \\ T_c = T - 2.0 \quad \text{for surface waters} & & \\ T_c = T - 1.3 \quad \text{for 0–50 m depth} & \text{(Weinelt } \textit{et al.}\text{, 1996)} & \\ \textit{Globigerina bulloides} & & \\ T_c = T - 1 & \text{(Duplessy } \textit{et al.}\text{, 1991)} & \end{array} \tag{3}$$

Any application of these relationships for estimating paleo-salinities must take into account the global changes of S and $\delta^{18}O_W$: (i) due to the sea level lowstand ($\Delta H \approx -100$m) during the Last Glacial Maximum the global salinity was increased by $\Delta S_{\Delta H} = 1.07$ psu (Fairbanks, 1989), and (ii) the oxygen isotopic composition of sea water was increased by $\Delta_{ICE} = 1.2‰$ because of the preferential storage of $H_2^{16}O$ in the ice sheets (Labeyrie *et al.*, 1987; Shackleton, 1987; Fairbanks, 1989). If no other changes had been present during the LGM, these global variations would simply shift (Fig. 8) the modern $\delta^{18}O_W$-S-relation (dashed line) to a glacial one with equal inclination (dotted line). However, additional non-global variations did most likely exist: From the sedimentary record we have strong evidence that the atmospheric and oceanic circulation patterns differed from the modern ones. This must have caused changes in evaporation and precipitiation and in the formation and melting of continental ice sheets, not only regarding the regions and intensities of these processes, but as well the temperatures at which the phase transitions took place. In other words, the freshwater $^{16}O/^{16}O$-fractionation might have been affected by non-global climatic changes. In fact, the greenland deep ice cores show glacial oxygen isotope ratios down to less than $-40‰$ (Dansgaard and Oeschger, 1989), which are substantially below the modern values around $-30‰$. This increase indicates a comparable glacial-to-present change of precipitating $\delta^{18}O$ that can be attributed to the lower air temperatures over the higher glacial ice dome (Craig and Gordon, 1965). However, the ice sheet models of Peltier (1994), Greve (1996), and Greve *et al.* (1996) reveal that during the LGM the Greenland ice cap was only a few meters higher than today. Thus the lower temperatures were the main cause for the $\delta^{18}O$ variations in ice and precipitation. Furthermore, the glacial temperatures were lower not only at the top of the ice dome but as well at sea level, and the $\delta^{18}O$ of marine precipitation must have been lower, too. This is confirmed by the atmospheric model results of Joussaume and Jouzel

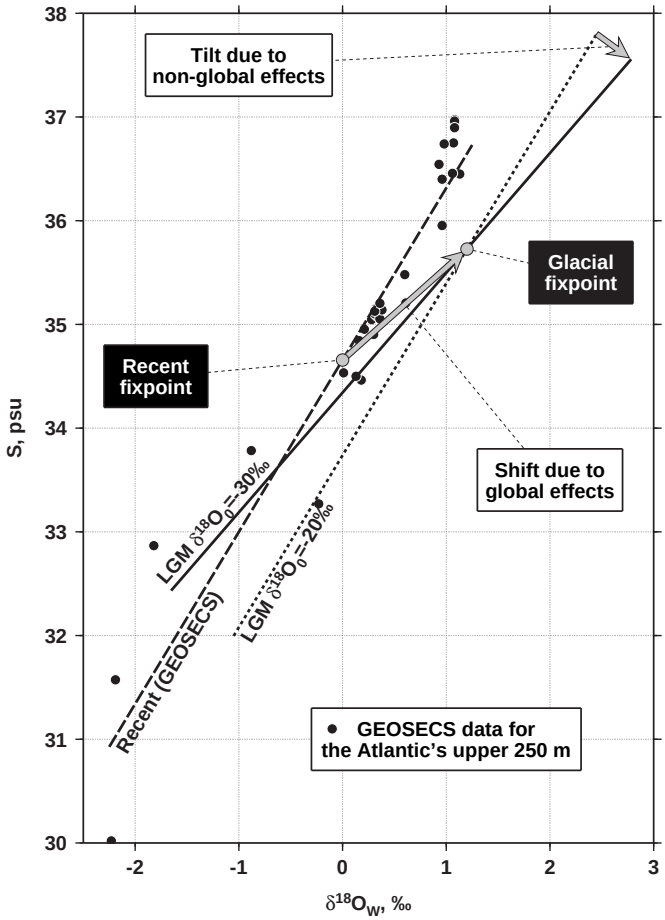

Figure 8: *Transformations between the recent (dashed line) and LGM (dotted and solid lines) $\delta^{18}O_W$ vs. S relationships. The global changes associated with sea level reduction and ice sheet buildup shift the modern (dashed) line by $\Delta_{ICE} = 1.2^0/_{00}$ and $\Delta S_{\Delta H} = 1.07$ psu to higher values (dotted). In addition, local changes as variations in oceanic and atmospheric circulation can tilt the relation (solid line).*

(1993) and Hoffmann (1995) that indicate a glacial high latitude lowering of rain and snow isotope ratios in the range of 5–$10^0/_{00}$. The isotopic composition of sea water, $\delta^{18}O_W$, strongly depends on the precipitated $\delta^{18}O$ (Craig and Gordon, 1965), so that these non-global variations very likely resulted in a reduced inclination of the glacial $\delta^{18}O_W$-S-relation (Fig. 8, solid line), that is, in an unknown $\mu^{LGM} < \mu^{rec}$.

Despite that, for all recent reconstructions of paleo-salinities (Duplessy *et al.*, 1991; Weinelt, 1993; Weinelt *et al.*, 1996) a value of $\mu^{LGM} = \mu^{rec} \approx 2$ has been adopted, yielding salinities almost coincident with the dotted line shown in Fig. 8. However, when I used these reconstructions for forcing SCINNA, the model results revealed severe physical inconsistencies already within the salinitiy field itself, but as well with the paleo-temperature data and the modelled circulation. Therefore I propose a modified approach for determining the glacial relationship between S and $\delta^{18}O_W$.

The assumptions underlying this approach are:

1. S and $\delta^{18}O_W$ were correlated linearly during the LGM. This is plausible since the LGM

lasted for a couple of millenia—in terms of atmospheric and oceanic timescales this can be be regarded as a stable climatic equilibrium. That is, any imprints of local $\delta^{18}O_0$ changes that might have initially bent the relation must have had enough time to be propagated all over the globe, thus producing a linear correlation in the Atlantic as it is the case today.

2. Apart from the sea level change ($\Delta S_{\Delta H}$) and the ice effect (Δ_{ICE}) there were no uniform global changes of S and $\delta^{18}O_W$.

3. The glacial S-$\delta^{18}O_W$-relation intersects the point marked by $S_0^{LGM} = S_0^{rec} + \Delta S_{\Delta H} = 35.73$ psu and $\delta^{18}O_W = \Delta_{ICE} = 1.2‰$, that is, the intercept of the modern (GEOSECS-) relation shifted by the two global effects, regardless of its slope (Fig. 8). The initial idea for fixing that point was to employ the (globally shifted) average sea surface salinities and isotope ratios. However, both values are highly variable and depend on the ocean area the average is computed for. For example, the mean annual surface salinity for the GIN Seas (between 45W/60N and 10E/80N) is 34.393 psu, whereas the slightly enlarged region 60W/50N to 15E/80N gives 35.518 psu (both values computed from the Levitus *et al.* (1994) dataset). Therefore the glacial fixpoint was based on the modern one from the GEOSECS data (Atlantic, uppermost 250 m).

4. The inclination of the S-$\delta^{18}O_W$-relation (μ^{LGM}) is controlled by the freshwater oxygen isotope ratio, $\delta^{18}O_0$, that may vary over a large range of values (from below $-40‰$ in the precipitation over the glacial ice caps to $\approx -10‰$ in recent rain), and thus is by far the most effective parameter for changing μ^{LGM} with respect to μ^{rec}.

5. The paleotemperature equation (2) is valid for the LGM, that is, the foraminiferan way of life did not change since then.

These assumptions yield a transformed version of equation (1) for the LGM:

$$[S - \Delta S_{\Delta H}] = S_0^{rec} + \mu^{LGM}\left[\delta^{18}O_W - \Delta_{ICE}\right], \quad \text{with} \quad \mu^{LGM} = -\frac{S_0^{rec}}{\delta^{18}O_0}, \tag{4}$$

or equivalently:

$$S = S_0^{rec}\left(1 - \frac{\delta^{18}O_W - \Delta_{ICE}}{\delta^{18}O_0}\right) + \Delta S_{\Delta H}, \tag{5}$$

with $\delta^{18}O_W$ to be computed from equation (2).

4 MODEL RESULTS

This section presents three salinity reconstructions based on different choices of $\delta^{18}O_0$ and the model results obtained with them:

Exp.	S_0^{rec} psu	$\delta^{18}O_0$ $^0/_{00}$	Ratio of $\delta^{18}O_W : S$	Remark
1.	34.45	-17.3	1 : 2.0	Relation taken from the LGM salinity reconstructions of Weinelt *et al.*, (1996). Resulting salinities: Fig. 9
2.	34.52	-20.0	1 : 1.7	Modern relation, after $\delta^{18}O_0 = -19.3^0/_{00}$ and $\delta^{18}O_W$:S = 1:1.79 from GEOSECS, (1987). Fig. 12
3.	34.52	-35.0	1 : 1.0	Extreme LGM test case. Fig. 14

For initialization of these experiments, the model was spun up for 400 years of integration time forced with an earlier glacial sea surface T and S reconstruction (Schäfer-Neth, 1994) that had been derived from the core-based temperature estimates by Schulz (1994; cf. Table 1, '94 T_{rek} data) and 131 $\delta^{18}O_C$ measurements with $\delta^{18}O_0 = -30^0/_{00}$ and the wind stress field introduced in the previous section. Starting with the three-dimensional circulation and T-S distribution from the end of this run, all other experiments described here were integrated with their respective surface T and S fields for further 400 years.

The T and $\delta^{18}O_C$ values used here pertain to summer, but dependable annual mean or even winter data are not yet available. Instead of using speculative winter data to fill in this gap, the LGM experiments were carried out under constant summer forcing. It has to be questioned whether driving a model perpetually with summer T and S yields reliable and significant results for the LGM. Indeed, forcing SCINNA permanently with the modern summer data produced a couple of irreal circulation features, such as a reversed East Greenland Current, whereas a perpetual winter forcing gives a realistic simulation (Fig. 6). The obvious reason for this is that at the present time the dominant forcing of the high latitudes takes place during the cold season: At a still ice-free sea surface, temperatures are low, wind speeds are high, and salinities are locally increased due to sea ice formation. The real ocean, too, could not develop its typical flow patterns and water mass distributions under permanent summer conditions, and in this sense the constant-summer model results are quite expectable.

As far as the glacial winter temperatures are concerned, some speculations can be made. Since it was colder during the LGM than today, the winter ice cover must have been more extensive, most likely reaching latitudes south of Iceland, somewhere between the summer and winter ice covers reconstructed by CLIMAP (1981). From these freezing conditions and the summer temperature reconstructions, a crude seasonal cycle or annual mean might be derived. However, there is yet no way of computing seasonal or annual mean salinities from these temperature assumptions and the summer $\delta^{18}O$ data. On the other hand, the large glacial winter ice cover yields a situation completely different from the modern one: Since the high-latitude ocean was isolated very efficiently from the atmosphere during the cold season, summer forcing must have been much more important during the LGM than today, at least for the high latitudes. Thus the results presented here should be regarded as an extreme glacial scenario, still subject to

reevaluation as soon as sufficient winter reconstructions become available.

4.1 Experiment 1

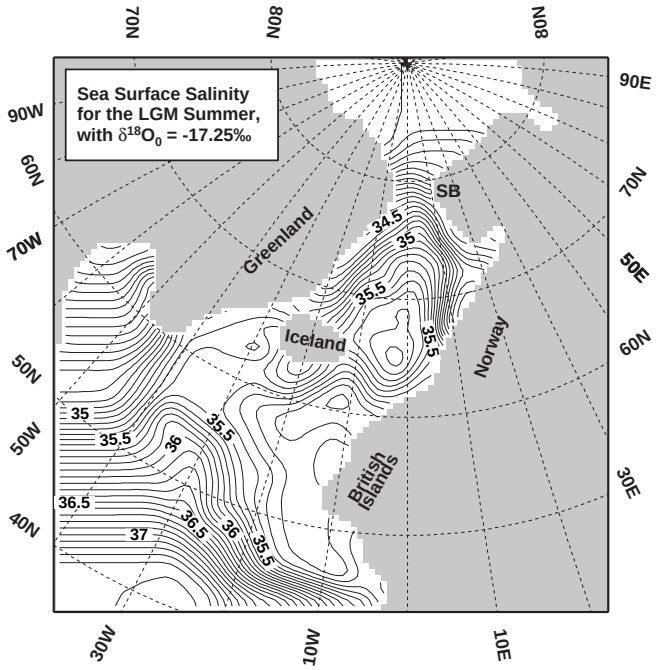

Figure 9: *Glacial sea surface salinity reconstruction computed from* $\delta^{18}O_W$ *with* $\delta^{18}O_0 = -17.3^0/_{00}$ *. Contour interval = 0.1 psu.*

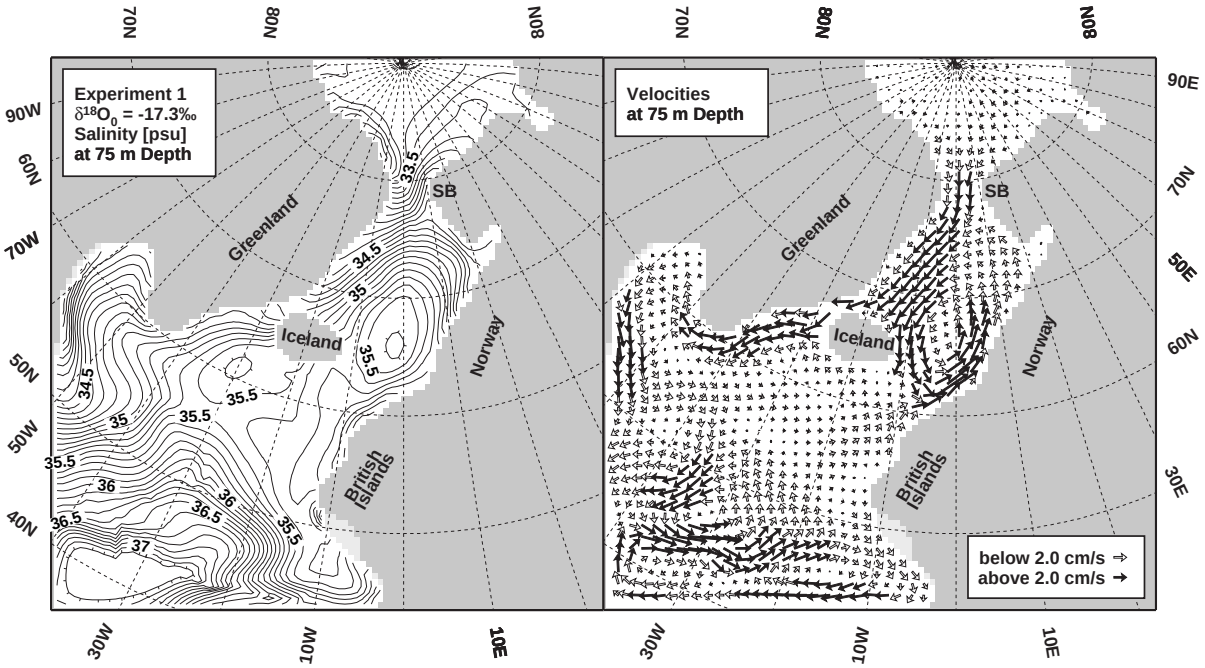

Figure 10: *Experiment 1 (*$\delta^{18}O_0 = -17.3^0/_{00}$ *): Salinitiy distribution and horizontal velocities at 75 m depth. Contour interval = 0.1 psu, scaling vectors = 2 cm/s.*

When computing S from the $\delta^{18}O_W$ field (Fig. 4) with $\delta^{18}O_W$:S = 1:2, the resulting salinity distribution (Fig. 9) exhibits a pronounced maximum of 35.7 psu at 3W/65N, separated by a sharp front from a low salinity region below 34.9 psu off Ireland and Great Britain. Along the

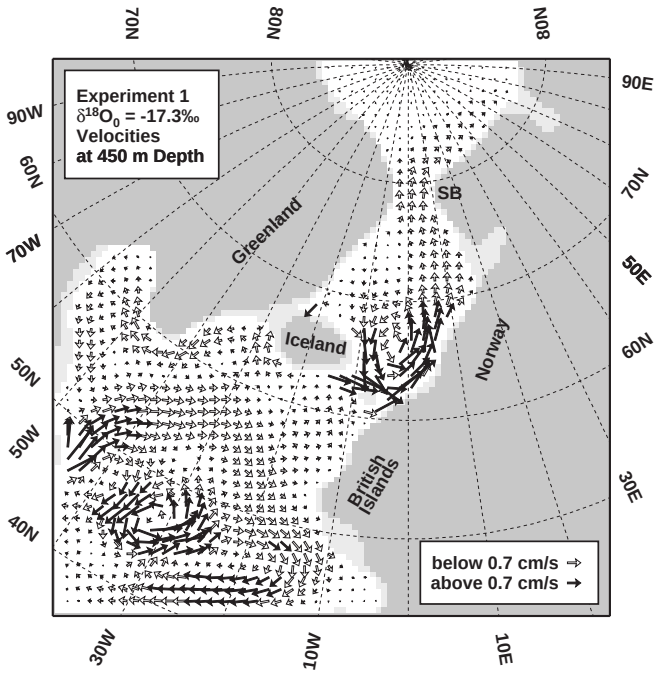

Figure 11: *Experiment 1 ($\delta^{18}O_0 = -17.3‰$): Horizontal velocities at 450 m depth. Scaling vectors = 0.7 cm/s.*

margins of the GIN Seas S has a minimum around 34 psu, thus indicating a cyclonal circulation. A tongue of high salinities (35.5–37 psu) spreads northward from the subtropics along 30W.

After reaching its steady state under this forcing, the circulation of the model's uppermost levels has developed an intense cyclone in the GIN Seas, shown here for the second level (centered at 75 depth; Fig. 10, right), that surrounds the salinity maximum (left). The western part of it feeds a glacial East Greenland Current and proceeds through the Denmark Strait into the Labrador Sea. These patterns are in accordance with both the wind field and the surface temperatures. On the other hand, there are severe discrepancies. The inflow into the GIN seas is confined to a narrow band at the coast of Scotland, transporting only approximately 35.1 psu, whereas the salinity in the GIN Seas rises to 35.6 psu and more. This contrast is even worse in the surface level. If we take the modern winter with its relatively warm and salty inflow sustaining somewhat lower T and S values in the GIN Seas as an analogue, we can conclude that this S reconstruction is not consistent with either the glacial temperatures, the wind field, or the modelled circulation. Another inconsistency of this type is revealed by the circulation at about 50N. The strong westerlies of the applied wind field and the T front along 45N should cause an anticylonal subtropical and a cyclonal subpolar gyre. However, the high salinity tongue at the surface produces an S maximum extending downward to more than 1000 m depth, thus inducing a completely different pattern. For example, at 450 m (Fig. 11) one finds a strong cyclone centered at 32W/47N, just below the tongue at the surface. This cyclone is surrounded by an anticyclonal current straddling the outer limits of the tongue. Again, the circulation is predominantly haline driven and completely different from what would be implied by T and wind

alone. In other words, the $\delta^{18}O_W$-S-Relation defined by $\delta^{18}O_0 = -17.3^0/_{00}$ is not appropriate for the LGM.

4.2 Experiment 2

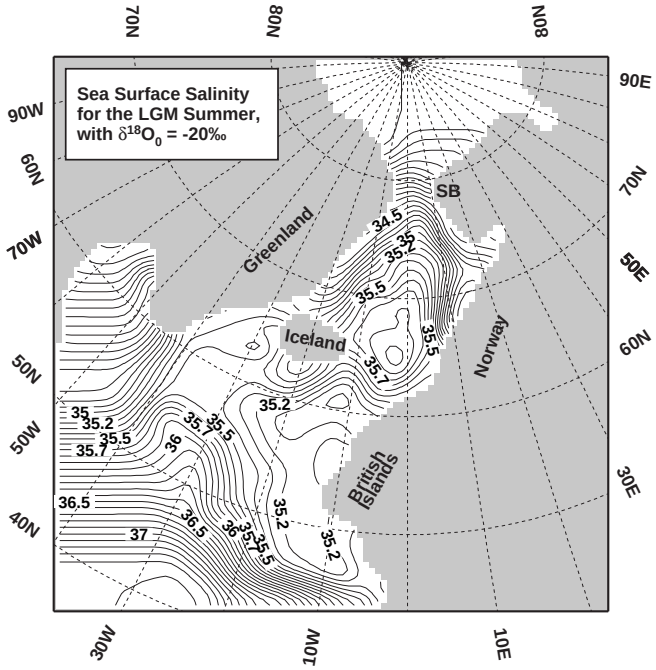

Figure 12: *Glacial sea surface salinity reconstruction computed from $\delta^{18}O_W$ with $\delta^{18}O_0 = -20^0/_{00}$. Contour interval = 0.1 psu.*

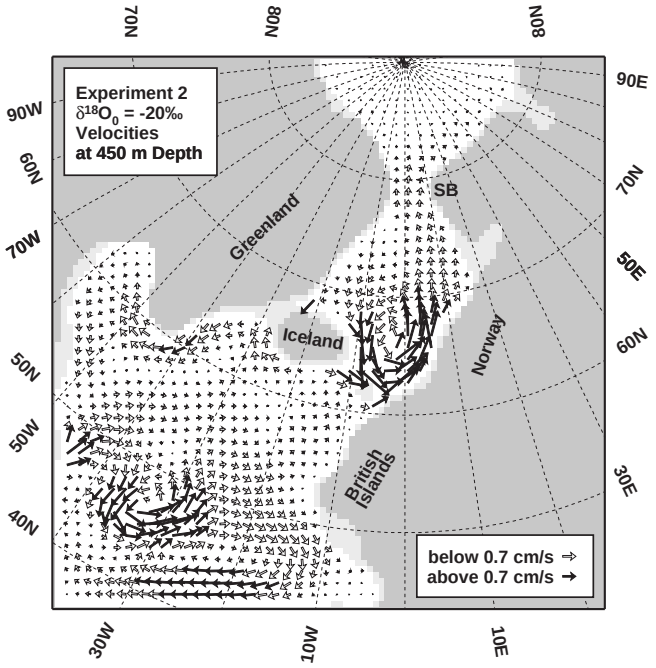

Figure 13: *Experiment 2 ($\delta^{18}O_0 = -20^0/_{00}$): Horizontal velocities at 450 m depth. Scaling vectors = 0.7 cm/s.*

Employing the GEOSECS value $\delta^{18}O_0 = -20^0/_{00}$ for computing S results in the glacial salinity distribution shown in Fig. 12. Compared to the first reconstruction (Fig. 9), S is about 0.2 psu

higher in and in the vicinity of the GIN Seas, with the maximum increased to 35.9 psu, and the minimum off Ireland and Scotland now being about 35.1 psu. In the subtropics, the salinities are lowered by 0.1 psu in the southwest corner of the model area. This yields a small overall reduction of the horizontal S gradients in the subtropic and subpolar regions, and essentially unchanged gradients in the GIN Seas.

Consequently, the modelled GIN Sea circulation and the overflows over the Greenland-Iceland-Scotland Ridge do not change with respect to experiment 1. But there are small changes in the area of the high salinity tongue. As can bee seen at 450 m depth (Fig. 13), there is some tendency to break the concentric cyclone and anticyclone centered at 32W/47N. Instead, the model tends to produce at least the aforementioned subtropical gyre, thus showing a better consistency between wind, thermal, and haline forcing.

4.3 Experiment 3

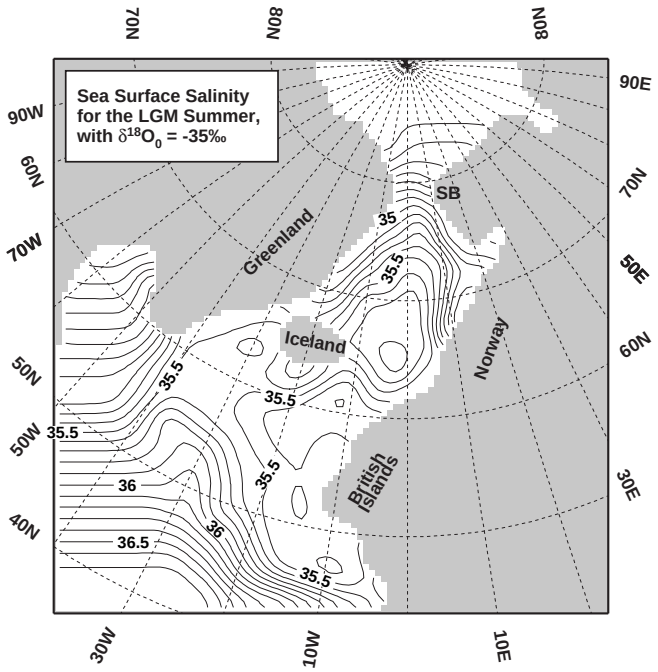

Figure 14: *Glacial sea surface salinity reconstruction computed from* $\delta^{18}O_W$ *with* $\delta^{18}O_0 = -35^0/_{00}$. *Contour interval = 0.1 psu.*

Obviously, the main flaw of the LGM salinity reconstructions discussed up to this point are too strong salinity gradients that produce currents conflicting with the thermal and the wind forcing. According to equation (5), one key to reduce S gradients is making $\delta^{18}O_0$ more negative. This is supported not only by the oxygen isotope measurements from the deep Greenland ice cores (Dansgaard and Oeschger, 1989), but as well by the atmospheric model results of Joussaume and Jouzel (1993) and Hoffmann (1995), that indicate a glacial high latitude lowering of $\delta^{18}O_0$ by approximately $10^0/_{00}$. As an extreme case, $\delta^{18}O_0 = -35^0/_{00}$ was used here to compute the sea surface salinities (Fig. 14) for the third experiment. At first glance it is clear that this choice reduces the salinity gradients considerably: The GIN Seas' maximum is 35.8 psu, dropping to

values around 35.1 psu along the coasts, the minimum values off Britain are increased to 35.4–35.5 psu, and the subtropical maximum is decreased by 0.7 psu to 36.7 psu.

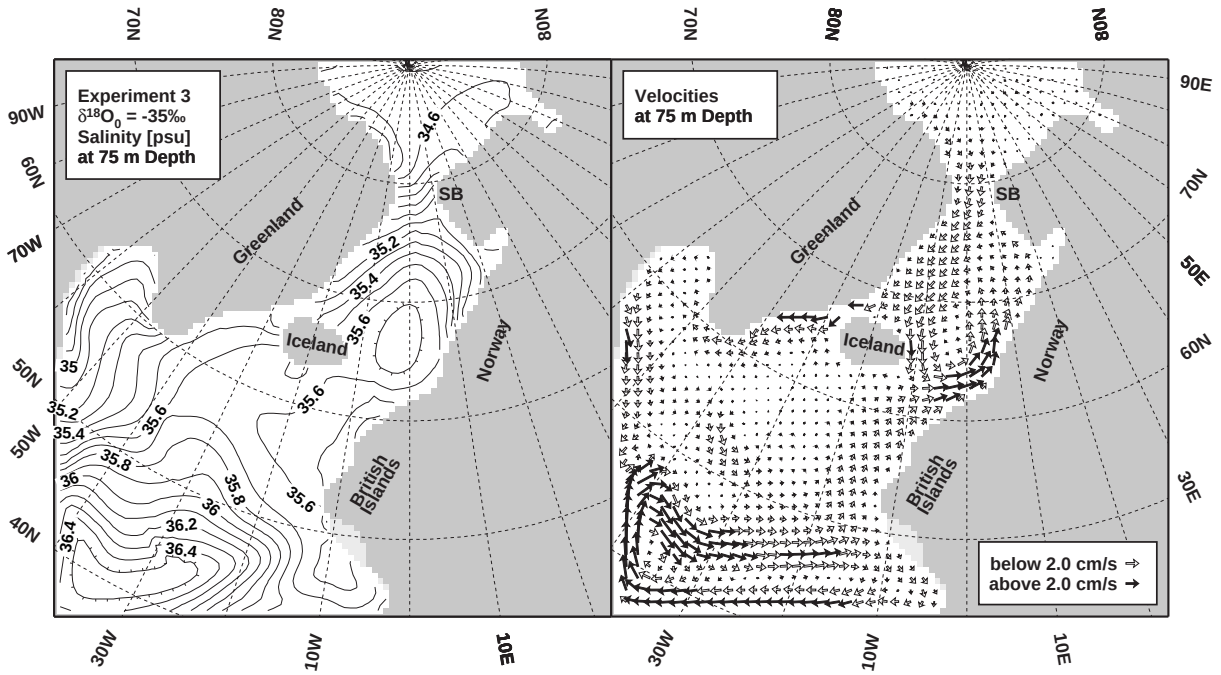

Figure 15: *Experiment 3 ($\delta^{18}O_0 = -35^0/_{00}$): Salinitiy distribution and horizontal velocities at 75 m depth. Contour interval = 0.1 psu, scaling vectors = 2 cm/s.*

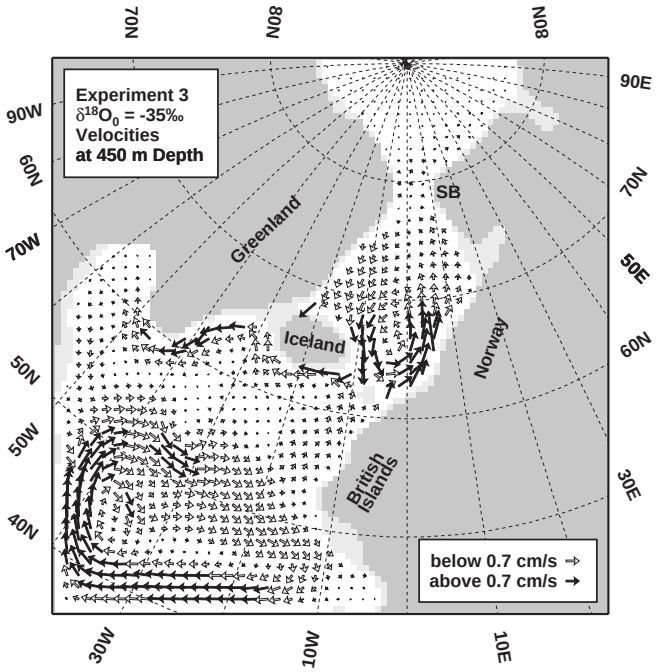

Figure 16: *Experiment 3 ($\delta^{18}O_0 = -35^0/_{00}$): Horizontal velocities at 450 m depth. Scaling vectors = 0.7 cm/s.*

The modelled near-surface circulation still presents (Fig. 15, right) the cyclone in the GIN Seas, the outflow through the Denmark Strait, and its continuation into the Labrador Basin. The inflow over the Iceland-Scotland Ridge is intensified and much wider than in the first two experiments.

Furthermore, it transports salinities around 35.6 psu (left), which is much closer to the values inside the GIN Seas (35.7 psu) than in the previously discussed model runs. This scenario is almost successful in maintaining the salt balance of this area, and this S field gives better results towards the subtropics, too. A distinct subtropical gyre has developed, although distorted by the southern model boundary, whose northern limit is shifted southward with respect to its modern location. This shift indepently confirms the model results of Seidov *et al.* (1996) that were based on a different approach for reconstructing paleo-salinities. Together with the currents south of Greenland and out of the Labrador Sea, the broad inflow into the GIN Seas branching off the subtropical gyre along the Irish/Bristish coast forms the subpolar cyclone missing from the two previous experiments. At 450 m depth (Fig. 16), the unrealistic cyclonal structure at 32W/47N has disappeared. In contrast to experiments 1 and 2, wich show an inflow into the GIN Seas both east and west of the Færøe Islands, this experiment gives an inflow only at the east side. West of the Færøes there is an outflow into the North Atlantic like nowadays, linked to deepwater formation north of the ridge. This is in good conceptual agreement with the results of Yu *et al.* (1996) who propose comparable meridional overturning rates for the Glacial and today based on radionuclide measurements.

5 CONCLUSIONS

From the numerical experiments discussed above, two main conclusions can be drawn:

1. Since the proxy data suggest that the glacial GIN Seas were free of ice during part of the seasonal cycle, these temperatures and the corresponding wind field imply a glacial circulation scheme quite similar to the modern one. Specifically the subpolar and subtropical gyres must have existed, and the high GIN Sea temperatures must have been maintained by a relatively warm inflow from the northeast Atlantic. Mainly due to the wind field, this inflow most likely went along the coast of Scotland. For the same reason, the East Greenland Current must have been present as well.

2. The combination of high $\delta^{18}O_C$ values and relatively high temperatures gives corresponding high salinities for the glacial GIN Seas, too, regardless of the specific S-$\delta^{18}O_W$ relationship. In parallel to the arguments regarding the temperatures, this requires a salty inflow from the Atlantic. On the other hand, the $\delta^{18}O_C$ values south of the Iceland-Scotland ridge are relatively low. If the modern relation between S and $\delta^{18}O_W$ is employed for calculating glacial salinities, the waters entering the GIN Seas do not carry enough salt to maintain the maximum in the interior. In other words, the horizontal salinity gradients are far too large. This applies also to the subpolar/subtropical region, where the steep S gradients cause a circulation inconsistent with the thermal and wind forcing. To avoid these strong gradients in spite of the high $\delta^{18}O_C$ differences, the modern S-$\delta^{18}O_W$ relation cannot be used for calculating glacial salinities. It must be replaced by an approximate 1:1 ratio. That is, a glacial fresh water oxyen isotope ratio

of $-30^0/_{00}$ or even less must be assumed, well below the modern value of $-20^0/_{00}$. Then the inconsistencies are minimized, and the resemblances between modern and glacial circulation that can be already deduced from the temperature distribution are strongly confirmed by the model results.

This glacial-to-modern $\delta^{18}O_0$ shift of more than $10^0/_{00}$ exceeds the $\delta^{18}O$ shift of precipitation (up to $10^0/_{00}$) that was obtained with atmospheric models (Joussaume and Jouzel, 1993; Hoffmann, 1995). One major reason for this are the high salinities reconstructed from the glacial summer temperatures that require a very low $\delta^{18}O_0$. When reliable winter and/or annual temperatures become available for the LGM, these lower temperatures will yield lower $\delta^{18}O_W$ values, too (cf. Eq. 2). Then, SCINNA can be expected to give consistent results with a higher glacial $\delta^{18}O_0$ than found in the present study, hence a better agreement of atmospheric and oceanic model results.

So far, a linear S-$\delta^{18}O_W$ relationship was employed for the whole model area, which might not appropriately represent the mixing of very different water masses in this region. To check this, a number of accompanying experiments was carried out where the value of $\delta^{18}O_0$ was changed (i) in the vicinity of the Greenland and Barents ice sheets from -$40^0/_{00}$ (glacier runoff) to -$15^0/_{00}$ (sea ice runoff) and (ii) in the region of inflow from the North Atlantic from -$30^0/_{00}$ (my LGM suggestion) to -$20^0/_{00}$ (modern value). These changes introduced additional gradients in the reconstructed salinity (and thus density) fields, causing quite different circulation changes.

Variations along the ice sheet margins mainly strengthen or weaken the boundary currents in the GIN Seas, without altering the circulation patterns very much. Because of this, and because of the very small effect of steady-state ice caps on $\delta^{18}O_0$ (Craig and Gordon, 1965), changes of this type were not further considered for this LGM study.

In contrast, changes in the inflow area lead to severe inconsistencies between (i) reconstructed sea surface salinity and modelled circulation and (ii) thermal and wind forcing. This finding could be expected: Recalling that the LGM was a stable climate state lasting for a couple of thousand years which is much longer than the overturning time scale of the global ocean, the low $\delta^{18}O$ entering the high latitudes by precipitation (Joussaume and Jouzel, 1993; Hoffmann, 1995) must have been propagated at least over the whole North Atlantic as it is the case today (GEOSECS, 1987), thereby removing local variations.

However, regional variations of the S-$\delta^{18}O_W$ relation should be considered in further experiments addressing the deglaciation phases that followed the LGM.

ACKNOWLEDGEMENTS

I thank G. Hoffmann for recomputing the glacial wind field, and K. Stattegger and D. Seidov for their comments that helped to improve the manuscript. The very constructive comments of two anonymous referees were greatly appreciated. This work was supported by the Deutsche Forschungsgemeinschaft within the framework of Sonderforschungsbereich 313, University Kiel.

REFERENCES

Bard, E., Arnold, M., Maurice, P., Duprat, J., and Duplessy, J.-C. (1987) Retreat Velocity of the North Atlantic Polar Front During the Last Deglaciation Determined by ^{14}C Accelerator Mass Spectrometry. *Nature*, 328: 791–794.

Bard, E., Hamelin, B., Fairbanks, R. G., and Zindler, A. (1990) Calibration of the ^{14}C Timescale Over the Past 30 000 Years Using Mass Spectrometric U-Th Ages from Barbados Corals. *Nature*, 345: 405–410.

Bond, G. C., and Lotti, R. (1995) Iceberg Discharges into the North Atlantic on Millenial Time Scales During the Last Glaciation. *Science*, 267: 1005–1009.

CLIMAP Project Members (1981) Seasonal Reconstructions of the Earth's Surface at the Last Glacial Maximium. *GSA Map and Chart Service*, MC-36 Boulder, Colorado: Geological Society of America.

Craig, H. and Gordon, L. I. (1965) Deuterium and Oxygen 18 Variations in the Ocean and the Marine Atmosphere. In *Stable Isotopes in Oceanographic Studies and Paleotemperatures* (E. Tongiorgi ed.) pp. 9–130. Pisa: Consiglio Nazionale delle Ricerche.

Dansgaard, W. and Oeschger, H. (1989) Past Environmental Long-Term Records from the Arctic. In *The Environmental Record in Glaciers and Ice Sheets* (H. Oeschger and C. C. Langway Jr. eds.) pp. 287–318. New York: Wiley.

Dietrich, G. (1969) Atlas of the Hydrography of the Northern North Atlantic. Charlottenlund Slot: Conseil International pour l'Exploration de la Mer, Service Hydrographique.

Duplessy, J.-C., Labeyrie, L., Juillet-Leclerc, A., Maitre, F., Duprat, J., and Sarnthein, M. (1991) Surface Salinity Reconstruction of the North Atlantic During the Last Glacial Maximum. *Oceanologica Acta*, 14: 311–324.

Duplessy, J.-C., Labeyrie, L., Arnold, M., Paterne, M., Duprat, J. and van Weering, T. C. E. (1992) Changes in Surface Salinity of the North Atlantic During the Last Deglaciation. *Nature* 358: 485–488.

Epstein, S., Buchsbaum, R., Lowenstam, H. A., and Urey, H. C. (1953) Revised Carbonate-Water Isotopic Temperature Scale. *Geological Society of America Bulletin*, 64: 1315–1325.

ETOPO5 (1986) Digital Relief of the Surface of the Earth. Boulder, Colorado: National Geophysical Data Center.

Fairbanks, R. G. (1989) A 17 000-Year Glacio-Eustatic Sea Level Record: Influence of Glacial Melting Rates on the Younger Dryas Event and Deep-Ocean Circulation. *Nature*, 342: 637–642.

GEOSECS (1987) Atlantic, Pacific, and Indian Ocean Expeditions: Shorebased Data and Graphics. In *GEOSECS Executive Committee* (H G. Östlund, H. Craig, W. S. Broecker and D. Spencer eds.) I.D.O.E., National Science Foundation, 7.

Greve, R. (1996) Application of a Polythermal Three-Dimensional Ice Sheet Model to the Greenland Ice Sheet: Response to Steady-State and Transient Climate Scenarios. *Journal of Climate*, in press.

Greve, R., Weis, M., and Hutter, K. (1996) Palaeoclimatic Evolution and Present Conditions of the Greenland Ice Sheet in the Vicinity of Summit: An Approach by Large-Scale Modelling. *Palaeoclimates*, submitted.

Haupt, B. J., Schäfer-Neth, C., and Stattegger, K. (1994) Modelling Sediment Drifts; A Coupled Oceanic Circulation-Sedimentation Model of the Northern North Atlantic. *Paleoceanography*, 9: 897–916.

Haupt, B. J., Schäfer-Neth, C., and Stattegger, K. (1995) Three-Dimensional Numerical Modelling of Late Quaternary Paleoceanography and Sedimentation in the Northern North Atlantic. *Geologische Rundschau*, 84: 137–150.

Hellerman, S. and Rosenstein, M. (1983) Normal Monthly Mean Wind Stress Over the World Ocean With Error Estimates. *Journal of Physical Oceanography*, 13: 1093–1104.

Hoffmann, G. (1995) Stabile Wasserisotopen im allgemeinen Zirkulationsmodell ECHAM. Hamburg, Germany: Max-Planck-Institut für Meteorologie, Examensarbeit 27, 98pp.

Jansen, E. and H. Erlenkeuser, H. (1985) Ocean Circulation in the Norwegian Sea 15 000 B.P. to Present. *Boreas*, 14: 189–206.

Jansen, E. and Veum, T. (1990) Evidence for Two-Step Deglaciation and its Impact on North Atlantic Deep Water Circulation. *Nature*, 343: 612–616.

Jones, G. A. and Keigwin, L. D. (1989) Evidence from Fram Strait (78 $^\circ$) for Early Deglaciation. *Nature*, 336: 56–59.

Joussaume, S. and Jouzel, J. (1993) Paleoclimatic Tracers: An Investigation Using an Atmospheric General Circulation Model Under Ice Age Conditions. 2. Water Isotopes. *Journal of Geophysical Research*, 98: 2807–2830.

Jünger, B. (1993) Tiefenwassererneuerung in der Grönlandsee während der letzten 340 000 Jahre. PhD Thesis, University of Kiel, Germany, 103pp.

Keigwin, L. D. and Boyle, E. A. (1989) Late Quaternary Chemistry of High-Latitude Surface Waters. *Paleogeography, Paleoclimatology, Paleoecology*, 3: 85–106.

Kellogg, T. B., Duplessy, J.-C., and N. Shackleton, N. (1978) Planctonic Foraminiferal and Oxygen Isotopic Stratigraphy and Paleoclimatology of Norwegian Deep-Sea Cores. *Boreas*, 7: 61–73.

Köhler, S. E. I. (1991) Spätquartäre paläo-ozeanographische Entwicklung des Nordpolarmeers anhand von Sauerstoff- und Kohlenstoffisotopenverhältnissen der planktischen Foraminifere Neogloboquadrina pachyderma (sin.). PhD Thesis, University of Kiel, Germany, 104pp.

Labeyrie, L. D., Duplessy, J.-C., and Blanc, P. L. (1987) Variations in Mode of Formation and Temperature of Oceanic Deep Water Over the past 125 000 Years. *Nature*, 327: 477–482.

Lackschewitz, K. S. (1991) Sedimentationsprozesse am aktiven mittelatlantischen Kolbinsey Rücken (nördlich von Island). PhD Thesis, University of Kiel, Germany, 121pp.

Lehman, S. J., Jones, G. A., Keigwin, L. D., Andersen, E. S., Butenko, G., and Østmo, S.-R. (1991) Initiation of Fennoscandian Ice-Sheet Retreat During the Last Deglaciation. *Nature*, 349: 513–516.

Levitus S., Burgett, R., Boyer, T. P. (1994) World Ocean Atlas 1994 Volume 3: Salinity. NOAA Atlas NESDIS 3. 99pp.

Mienert, J., Andrews, J. T., and Milliman, J. D., (1992) The East Greenland Continental Margin (65 ° N) Since the Last Deglaciation: Changes in Seafloor Properties and Ocean Circulation. *Marine Geology*, 106: 217–238.

Morris, T. H. (1988) Stable Isotope Stratigraphy of the Arctic Ocean: Fram Strait to Central Arctic. *Paleogeography, Paleoclimatology, Paleoecology*, 64: 201–219.

Pacanowski, R., Dixon, K. D., and Rosati, A. (1993) The G.F.D.L Modular Ocean Model Users Guide. *GFDL Ocean Group Technical Report No. 2*, Geophysical Fluid Dynamics Laboratory / NOAA, Princeton University.

Peltier, W. R. (1994) Ice Age Paleotopography. *Science*, 265: 195–201.

Pflaumann, U., Duprat, J., Pujol, C, and Labeyrie, L. (1996) SIMMAX, a Transfer Technique to Deduce Atlantic Sea Surface Temperatures from Planctonic Foraminifera — the "EPOCH" Approach. *Paleoceanography*, 11: 15–35.

Ruddiman, W. F. and A. McIntyre, A. (1981) The North Atlantic During the Last Deglaciation. *Paleogeography, Paleoclimatology, Paleoecology*, 35: 145–214.

Sarnthein, M., Jansen, E., Weinelt, M., Arnold, M., Duplessy, J.-C., Erlenkeuser, H., Flatøy, A., Johannessen, G., Johannessen, T., Jung, S., Koc, N., Labyerie, L., Maslin, M., Pflaumann, U., and Schulz, H. (1995) Variations in Atlantic Surface Ocean Paleoceanography, 50 ° – 85 ° N: A Time-Slice Record of the Last 55 000 Years. *Paleoceanography*, 10: 1063–1094.

Schäfer-Neth, C. (1994) Modellierung der Paläoozeanographie des nördlichen Nordatlantiks zur Zeit der letzten Maximalvereisung. PhD Thesis, University of Kiel, Germany, 105pp.

Schäfer-Neth, C. and Stattegger, K. (1996) Meltwater Pulses in the Northern North Atlantic: Retrodiction and Forecast by Numerical Modelling. *Geologische Rundschau*, in press.

Schulz, H. (1994) Meeresoberflächentemperaturen im Nordatlantik und in der Norwegisch-Grönländischen See vor 9 000 Jahren. Auswirkungen des frühholozänen Insolationsmaximums, PhD Thesis, University of Kiel, Germany, 119pp.

Seidov, D., Sarnthein, M., Stattegger, K., Prien, R., and Weinelt, M. (1996) North Atlantic Ocean Circulation During the Lat Glacial Maximum and Subsequent Meltwater Event: A Numerical Model. *Journal of Geophysical Research*, 101: 16 305–16 332.

Shackleton, N. J. (1974) Attainment of Isotopic Equlibrium Between Ocean Water and the Benthonic Foraminifera Uvigerina: Isotopic Changes in the Ocean During the Last Glacial. *Colloque CNRS n° 219* pp. 203–210 Paris: Centre National de la Recherche Scientifique.

Shackleton, N. J. (1987) Oxygen Isotopes, Ice Volume, and Sea Level. *Quaternary Science Review*, 6: 183–190.

Veum, T., Arnold, M., Beyer, I., and Duplessy, J.-C., (1992) Water Mass Exchange Between the North Atlantic and the Norwegian Sea During the Last 28 000 Years. *Nature*, 356: 783–785.

Vogelsang, E. (1990) Paläo-Ozeanographie des Europäischen Nordmeers an Hand stabiler Kohlenstoff- und Sauerstoffisotopen PhD Thesis, University of Kiel, Germany, 136pp.

Wadhams, P. (1986) The ice cover. In *The Nordic Seas* (B. G. Hurdle ed.) pp. 21–87. New York: Springer.

Weinelt, M. S. (1993) Veränderungen der Oberflächenzirkulation im Europäischen Nordmeer während der letzten 60 000 Jahre — Hinweise aus stabilen Isotopen. PhD Thesis, University of Kiel, Germany, 106pp.

Weinelt, M., Sarnthein, M., Pflaumann, U., Schulz, H., Jung, S., and Erlenkeuser, H., (1996) Ice-Free Nordic Seas During the Last Glacial Maximum? Potential Sites of Deepwater Formation. *Paleoclimates*, 3: 23–57.

Wessel, P. and Smith, W. H. F. (1991) Free Software Helps Map and Display Data. *EOS Transactions AGU*, 72: 441, 445–446.

Yu, E.-F., Francois, R., and Bacon, M. P. (1996) Similar Rates of Modern and Last-Glacial Ocean Thermohaline Circulation Inferred from Radiochemical Data. *Nature*, 379: 689–694.

Zahn, R., Markussen, B., and Thiede, J. (1985) Stable Isotope Data and Depositional Environments in the Late Qauternary. *Nature*, 314: 433–435.

Zahn, R. and Mix, A. C. (1991) Benthic Foraminiferal δ^{18}O in the Ocean's Temperature-Salinity-Density Field: Constraints on Ice Age Thermohaline Circulation. *Paleoceanography*, 6: 1–20.

APPENDIX

Table 1: Core data used for this study.

Core	$\delta^{18}O_C$ Source	Spe-cies	Location Lon.	Lat.	$\delta^{18}O_C$ PDB	T_{rek}/ ° C '96	'94	T_{int} ° C	$\delta^{18}O_W$ SMOW
1171	19	pa.	-18.07	68.20	4.49	3.0		2.62	0.85
BOFS 5K	19	pa.	-21.87	50.68	4.17	4.3		4.46	1.04
BOFS 8K	19	pa.	-22.04	52.50	4.21	3.8	4.0	4.02	0.96
BOFS 14K	19	pa.	-19.44	58.62	4.11	3.6	4.4	3.69	0.77
BOFS 17K	19	pa.	-16.50	58.00	4.17	3.6	4.4	3.70	0.83
CH 66-03	11	pa.	-2.18	44.08	3.41			6.62	0.85
CH 67-19	11	pa.	-3.95	45.75	3.57			6.44	0.97
CH 69-09	11	bu.	-47.35	41.75	3.17			10.28	1.63
CH 69-12	11	pa.	-4.69	46.02	3.65			6.46	1.05
CH 69-32	11	pa.	-5.18	45.40	3.56			6.67	1.02
CH 69-69	11	pa.	-4.51	43.84	3.66			7.20	1.25
CH 72-101	11	pa.	-8.56	47.47	3.51			6.40	0.90
CH 72-104	11	pa.	-8.08	46.90	3.25			6.50	0.66
CH 73-108	11	pa.	-10.73	58.08	4.18			4.04	0.93
CH 73-110	17	pa.	-8.93	59.50	4.00			3.99	0.74
CH 73-136	8	pa.	-14.47	55.57	4.18			3.98	0.92
CH 73-139	5	pa.	-16.35	54.64	3.99			4.40	0.84
CH 73-141	11	pa.	-16.52	52.86	4.00			4.40	0.85
CH 77-07	2	pa.	-10.52	66.60	4.72			3.20	1.25
FRAM 1/4	4	pa.	-8.95	84.50	4.69			-1.90	-0.25
FRAM 1/7	4	pa.	-6.96	83.88	4.60			-1.90	-0.34
HM 1007	18	pa.	-4.72	61.67	4.44			3.72	1.11
HM 52-43	13	pa.	0.73	64.25	4.51			3.31	1.07
HM 57-07	18	pa.	-13.53	68.25	4.48			3.01	0.95
HM 71-12	18	pa.	-13.87	68.43	4.73			2.96	1.19
HM 71-14	18	pa.	-18.08	69.83	4.65			1.34	0.66
HM 71-19	18	pa.	-9.51	69.48	4.81			3.00	1.28
HM 80-42	18	pa.	-9.23	72.25	4.51			2.40	0.81
HM 80-60	18	pa.	-11.86	68.90	4.69			2.99	1.16
HM 94-13	18	pa.	-1.62	71.63	4.66			2.79	1.07
HM 94-18	18	pa.	5.70	74.50	4.57			2.53	0.91
HM 94-25	18	pa.	1.32	75.60	4.68			2.06	0.89
HM 94-34	18	pa.	-2.54	73.77	4.80			2.41	1.11
HU 75-37	11	pa.	-48.38	59.15	4.40			0.76	0.24
HU 75-41	11	pa.	-53.86	62.65	4.89			-0.68	0.31
HU 75-42	11	pa.	-53.89	62.65	4.75			-0.69	0.17
HU 75-58	11	pa.	-59.37	62.78	4.53			-1.33	-0.24
K 11	2	pa.	1.60	71.78	4.66			2.77	1.07
KN 708-1	19	pa.	-23.75	50.00	4.16	4.1	5.1	4.74	1.11
KN 708-6	11	pa.	-29.57	51.57	4.46			5.20	1.53

Table 1 (continued): Core data used for this study.

Core	$\delta^{18}O_C$ Source	Spe- cies	Location Lon.	Lat.	$\delta^{18}O_C$ PDB	T_{rek}/ °C '96	'94	T_{int} °C	$\delta^{18}O_W$ SMOW
KN 714-15	8	pa.	-25.95	58.77	4.23			3.66	0.88
M 15637	11	bu.	-18.98	27.00	1.89			19.70	2.57
M 15672	11	bu.	-8.13	34.87	2.32			14.12	1.71
M 17045	18	pa.	-16.65	52.43	4.01	3.9		4.38	0.86
M 17048	18	pa.	-18.16	54.30	4.02			4.58	0.92
M 17049	18	pa.	-26.73	55.28	4.29	4.0	4.4	4.06	1.05
M 17051	19	pa.	-31.98	56.17	4.34	3.9		3.89	1.05
M 17701	9	pa.	11.68	68.53	4.34			0.80	0.19
M 17719	17	pa.	12.57	72.15	4.39			1.69	0.49
M 17724	17	pa.	8.33	76.00	4.63	2.6		1.66	0.73
M 17725	17	pa.	4.58	77.47	4.41	3.0	3.8	1.83	0.55
M 17728	17	pa.	3.95	76.52	4.69			2.08	0.90
M 17730	17	pa.	7.31	72.05	4.60	2.7	3.2	2.48	0.92
M 17732	17	pa.	4.23	71.62	4.75			2.73	1.15
M 23041	6	pa.	0.22	68.68	4.75			3.24	1.29
M 23043	10	pa.	-3.35	70.27	4.57			2.99	1.04
M 23055	10	pa.	4.01	68.42	4.76			3.06	1.25
M 23056	19	pa.	3.83	68.50	4.71	3.9		3.09	1.20
M 23057	10	pa.	3.31	68.40	4.70			3.15	1.21
M 23059	10	pa.	-3.12	70.30	4.72			2.98	1.19
M 23062	10	pa.	0.16	68.73	4.73			3.24	1.26
M 23063	10	pa.	0.00	68.75	4.76			3.23	1.29
M 23064	10	pa.	0.33	68.67	4.66			3.24	1.20
M 23065	10	pa.	0.81	68.50	4.80	3.3	4.9	3.26	1.34
M 23068	10	pa.	1.50	67.83	4.74			3.23	1.27
M 23071	10	pa.	2.93	67.08	4.73	2.8	3.6	3.06	1.22
M 23074	10	pa.	4.92	66.67	4.96	2.9		2.80	1.37
M 23254	17	pa.	9.63	73.12	4.70			2.42	1.01
M 23256	17	pa.	10.95	73.18	4.73			2.18	0.97
M 23258	17	pa.	13.98	75.00	4.52			-0.12	0.11
M 23259	17	pa.	9.25	72.03	4.68			2.22	0.93
M 23260	17	pa.	11.46	72.13	4.71			1.92	0.88
M 23261	17	pa.	13.11	72.17	4.60			1.55	0.66
M 23262	17	pa.	14.43	72.23	4.33	2.7		1.12	0.27
M 23269	17	pa.	0.68	71.45	4.83			2.82	1.25
M 23294	17	pa.	-10.59	72.37	4.71	2.6		2.12	0.94
M 23323	9	pa.	5.93	67.77	4.42			2.55	0.76
M 23419	19	pa.	-19.74	54.97	3.96	5.1		4.67	0.88
MG 123	6	pa.	0.81	79.27	4.65			0.22	0.34
NA 87-22	14	pa.	-14.57	55.50	4.15	3.7	4.8	4.00	0.90

Table 1 (continued): Core data used for this study.

Core	$\delta^{18}O_C$ Source	Species	Location Lon.	Lat.	$\delta^{18}O_C$ PDB	T_{rek}/ °C '96	'94	T_{int} °C	$\delta^{18}O_W$ SMOW
NO 77-14	11	pa.	-20.42	62.45	4.65			3.71	1.31
NO 79-06	11	pa.	-36.89	54.52	4.76			3.60	1.40
NO 79-17	11	bu.	-27.17	43.01	3.23			12.67	2.27
NO 79-25	11	pa.	-27.28	46.98	4.10			7.28	1.72
NO 79-29	11	bu.	-15.07	46.30	3.23			7.19	0.90
ODP 646	11	pa.	-48.92	58.22	4.42			0.89	0.30
ODP 647	11	pa.	-45.26	53.33	4.19			2.63	0.56
POS 0006	12	pa.	-16.82	69.20	4.43			2.15	0.66
POS 0020	12	pa.	-18.54	67.98	4.49			2.71	0.88
POS 16343	9	pa.	7.46	66.93	4.33			2.30	0.61
POS 16396	18	pa.	-11.25	61.87	4.08	3.5	3.8	3.55	0.70
PS 21291	17	pa.	8.07	78.00	4.54			1.03	0.46
PS 21295	7	pa.	-2.43	78.00	4.63			0.57	0.42
PS 21535	15	pa.	1.85	78.75	4.73			0.84	0.59
PS 21736	16	pa.	-5.17	74.33	4.65			1.83	0.79
PS 21842	18	pa.	-16.52	69.45	4.48			2.05	0.69
PS 21900	16	pa.	-2.32	74.53	4.45			2.11	0.67
PS 21906	18	pa.	-2.10	76.50	4.56			1.35	0.57
PS 21910	18	pa.	1.32	75.62	4.60			2.06	0.81
PS 23199	10	pa.	5.24	68.38	4.77			2.76	1.17
PS 23205	10	pa.	5.76	67.62	4.62			2.60	0.98
PS 23243	10	pa.	-6.54	69.38	4.71			3.07	1.20
PS 23246	10	pa.	-12.86	69.40	4.58			2.82	1.00
RC 9-225	11	pa.	-15.40	54.89	3.99			4.23	0.80
S 8-79-04	11	bu.	-22.00	42.00	2.87			14.06	2.24
SU 81-14	11	bu.	-9.86	36.77	2.52			14.42	1.98
SU 81-18	11	bu.	-10.34	37.77	2.32			14.00	1.68
SU 81-32	11	bu.	-9.78	42.10	3.27			9.83	1.61
SU 81-47	11	pa.	-3.30	44.88	3.44			6.57	0.87
SU 90 I06	19	pa.	-39.45	59.98	4.57	3.3		3.00	1.04
SU 90 I07	18	pa.	-28.08	63.08	4.17			3.35	0.74
UB 25-09	3	pa.	4.79	63.05	4.49			3.02	0.96
UB 31-33	3	pa.	1.78	63.63	4.44			3.36	1.01
UB 31-36	3	pa.	0.53	64.25	4.88			3.31	1.44
V 23-23	11	pa.	-44.55	56.08	4.34			2.45	0.66
V 23-42	8	pa.	-27.92	62.18	4.52			3.40	1.10
V 23-81	9	pa.	-16.14	54.03	4.02	4.7	5.2	4.47	0.89
V 23-82	11	pa.	-21.93	52.59	4.34			4.03	1.09
V 23-83	8	pa.	-24.26	49.87	4.31			4.84	1.28
V 27-17	11	pa.	-37.31	50.08	4.42			4.38	1.27

Table 1 (end): Core data used for this study.

Core	$\delta^{18}O_C$ Source	Species	Location Lon.	Location Lat.	$\delta^{18}O_C$ PDB	T_{rek}/ °C '96	T_{rek}/ °C '94	T_{int} °C	$\delta^{18}O_W$ SMOW
V 27-19	11	pa.	-38.79	52.10	4.46			3.77	1.14
V 27-20	11	pa.	-46.20	54.00	4.33			2.40	0.63
V 27-60	11	pa.	8.58	72.17	4.72			2.36	1.01
V 27-86	8	pa.	1.13	66.60	4.72	3.3	2.8	3.16	1.23
V 27-114	8	pa.	-33.08	55.05	4.42			4.01	1.17
V 27-116	11	pa.	-30.33	52.83	4.52			4.79	1.48
V 28-14	1	pa.	-29.58	64.78	4.60	3.2	4.0	3.07	1.09
V 28-38	8	pa.	-4.40	69.38	4.82			3.10	1.32
V 28-56	1	pa.	-6.12	68.03	4.67		3.5	3.17	1.19
V 29-180	11	pa.	-23.87	45.30	3.80			8.89	1.83
V 29-183	8	pa.	-25.50	49.14	4.10			5.57	1.27
V 30-108	8	pa.	-38.73	56.10	4.52			3.18	1.04
V 30-164	11	pa.	8.97	69.83	4.83			1.34	0.83

Notes on Table 1:

1. $\delta^{18}O_C$ sources: 1: Kellogg et al. (1978); 2: Ruddiman and McIntyre (1981); 3: Jansen and Erlenkeuser (1985); 4: Zahn et al. (1985); 5: Bard et al. (1987); 6: Morris (1988); 7: Jones and Keigwin (1989); 8: Keigwin and Boyle (1989); 9: Jansen and Veum (1990); 10: Vogelsang (1990); 11: Duplessy et al. (1991); 12: Lackschewitz (1991); 13: Veum et al. (1992); 14: Duplessy et al. (1992); 15: Köhler (1991); 16: Jünger (1993); 17: Weinelt (1993); 18: Sarnthein et al. (1995); 19: Weinelt et al. (1996).

2. Foraminifer species: pa. = *Neogloboquadrina pachyderma sin.*, bu. = *Globigerina bulloides.*

3. $\delta^{18}O_C$: Glacial oxygen isotope ratio (PDB) of fossil foraminifer shells.

4. T_{rek}: Temperature reconstructed from faunal assemblages: '96: Weinelt et al. (1996); '94: Older reconstructions by Schulz (1994) that were used for modeling the glacial wind field (Hoffmann, 1996, pers. comm.).

5. T_{int}: Temperatures interpolated from the model surface forcing set (Fig. 3) to the core locations.

6. $\delta^{18}O_W$: Isotopic composition of sea water (SMOW), computed from $\delta^{18}O_C$ and T_{int} by means of equation (2).